



RELAXATION IN SHAPE-MEMORY ALLOYS—PART II. THERMO-MECHANICAL MODEL AND PROPOSED EXPERIMENTS

K. BHATTACHARYA¹†, R. D. JAMES² and P. J. SWART³

¹Division of Engineering and Applied Science, 104-44 California Institute of Technology, Pasadena, CA 91125, ²Department of Aerospace Engineering and Mechanics, University of Minnesota, Minneapolis, MN 55455, and ³Theoretical Division, MS-B284, Los Alamos National Laboratory, Los Alamos, NM 87545, U.S.A.

(Received 12 November 1996; accepted 27 March 1997)

Abstract—A variety of relaxation phenomena such as stabilization of martensite, rubber-like behavior, evolving hysteresis loops and stabilization of interfaces have been observed in various shape-memory alloys. These effects adversely impact technological applications. In Part I of this paper we proposed a phenomenological, but predictive, model of the mechanical behavior of these materials. We showed that this model reproduces the experimental observations. In this part, we extend this model to include the effects of temperature and the austenite–martensite transformation. Once again, the predictions from this extended model agree with experimental observations. We can therefore conclude that the basic phenomenological ideas combined with a few easily measured material parameters is sufficient to predict the behavior of these materials. Finally, we propose new experiments in order to probe longstanding issues concerning the mechanism responsible for the relaxation. © 1997 Acta Metallurgica Inc.

1. INTRODUCTION

A variety of relaxation phenomena such as stabilization of martensite, rubber-like behavior, evolving hysteresis loops and stabilization of interfaces have been observed in various shape-memory alloys. These effects adversely impact technological applications. In Part I [1] of this paper (henceforth referred to as Part I) we proposed a phenomenological, but predictive, model of the mechanical behavior of these materials. The model and the important material parameters are summarized at the end of Section 4 in that paper. In Section 2 below, we extend the model to include temperature changes and the austenite–martensite transformation. In particular, we examine the effect of various thermomechanical histories on the migration of the austenite–martensite transformation temperature. We show that the predictions agree with experimental observations. Finally, we use the model in Section 3 to design new experiments in

2. STABILIZATION OF MARTENSITE

In this section we extend the energy introduced in Section 3 of Part I to temperatures above the martensitic transformation temperature. We write down an energy suitable for a material undergoing transformation from a high temperature “austenite” phase to a low temperature “martensite” phase with two variants, “+” and “−”. The austenite has preferred strain and shift $\{0, 0\}$ while the martensite variants have preferred strain and shift $\{\epsilon^+, 1\}$ and $\{\epsilon^-, -1\}$, with $\epsilon^+ > 0 > \epsilon^-$. We assume the existence of a temperature θ_0 such that the free energy per unit reference volume $\varphi(\epsilon, p, \theta)$ satisfies

$$\begin{aligned} \varphi(0, 0, \theta) &< \varphi(\epsilon, p, \theta) \quad \text{if } \theta > \theta_0, \\ \varphi(\epsilon^+, 1, \theta) = \varphi(\epsilon^-, -1, \theta) &< \varphi(\epsilon, p, \theta) \\ &\text{if } \theta < \theta_0. \end{aligned} \quad (2.1)$$

We do all our calculations with the energy

$$\varphi(\epsilon, p, \theta) = \frac{1}{2} \min \left\{ \begin{aligned} &\alpha(\epsilon - \epsilon^+)^2 + 2\delta(\epsilon - \epsilon^+)(p - 1) + \beta(p - 1)^2 + 2\lambda_m(\theta - \theta_0), \\ &\alpha(\epsilon - \epsilon^-)^2 + 2\delta(\epsilon - \epsilon^-)(p + 1) + \beta(p + 1)^2 + 2\lambda_m(\theta - \theta_0), \\ &\alpha\epsilon^2 + 2\delta\epsilon p + \beta p^2 + 2\lambda_a(\theta - \theta_0) \end{aligned} \right\} \quad (2.2)$$

order to further understand longstanding issues concerning the mechanism responsible for the relaxation.

which is the minimum of three quadratic wells whose depths depend linearly on temperature. We define

†To whom all correspondence should be addressed.

$$\lambda = \lambda_m - \lambda_a; \quad (2.3)$$

λ is the latent heat of transformation and we assume that it is positive. Notice that we have assumed for simplicity that the moduli are the same for the austenite as well as for both the variants of martensite.

As in Part I, we shall use α , $B = \beta - \delta^2/\alpha$ and $D = \delta/\alpha$ (respectively, the elastic modulus, the normalized shift modulus and the normalized coupling modulus) as the material parameters to be determined from experiment. However, we retain ϵ^+ , ϵ^- rather than combining them in $\epsilon_T = \epsilon^+ + \epsilon^- + 2D$.

Assume that the bar is immersed in a heat bath of temperature $\theta(t)$ and subject to an applied load $F(t)$. As in Part I, equation (3.6), we let $\sigma(x, t) = F(t)/A(x)$ and define the total energy by,

$$\int_0^L A(x) \{ \varphi(\epsilon(x, t), p(x, t), \theta(t)) - \sigma(x, t)\epsilon(x, t) \} dx. \tag{2.4}$$

Note that we have implicitly assumed that the temperature is uniform in the bar and is equal to the temperature of the heat bath at each time. This is reasonable if the time required for the bar to attain thermal equilibrium is much smaller than the typical processes (relaxation) that we wish to study.

Based on this energy we write down a model analogous to that of Part I, Section 4. There, we wrote down a model based on energy minimization, but then slightly modified it by adding an "inherent hysteresis" σ_{st} . For simplicity, in this section we

confine ourselves to the energy minimization and do not add inherent hysteresis.

For a prescribed load $F(t)$, temperature $\theta(t)$ and initial distribution of shift $p_0(x)$ and strain $\epsilon_0(x)$, the functions $u(x, t)$ and $p(x, t)$ are determined by

$$\begin{aligned} \text{(i)} \quad & \min_{u(0,t)=0} \int_0^L A(x) \{ \varphi(\epsilon(x, t), p(x, t), \theta(t)) \\ & - \sigma(x, t)\epsilon(x, t) \} dx \quad \text{at each } t, \\ \text{(ii)} \quad & \frac{\partial p}{\partial t}(x, t) = -\mu \frac{\partial \varphi}{\partial p}(\epsilon(x, t), p(x, t), \theta(t)), \\ \text{(iii)} \quad & p(x, 0) = p_0(x), \quad \epsilon(x, 0) = \epsilon_0(x), \quad 0 \leq x \leq L. \end{aligned} \tag{2.5}$$

Here, as before, $\mu > 0$ is the mobility, and the minimization problem is interpreted as in Part I.

We now specialize to the energy (2.2) and describe the solution procedure, which is analogous to that of Section 4 of Part I. We begin with (2.5), for a given t and $p(x, t)$. In order to minimize the total energy, we choose a strain that minimizes the integrand at each x . Thus, for a given t and x , we choose $\epsilon(x, t)$ to minimize $f(\epsilon) = \varphi(\epsilon, p(x, t), \theta(t)) - \sigma(x, t)\epsilon$. Since, φ has a triple-well structure, the equation $(\partial \varphi / \partial \epsilon) = 0$ has three solutions: $\epsilon = \epsilon^+ + \sigma/\alpha - D(p - 1)$, $\epsilon = \epsilon^- + \sigma/\alpha - D(p + 1)$ and $\epsilon = \sigma/\alpha - Dp$. By comparing the values of f on these three solutions we conclude that

$$\epsilon(x, t) = \begin{cases} \epsilon^- + \frac{\sigma(x, t)}{\alpha} - D(p(x, t) + 1) & \text{if } \{p(x, t), \sigma(x, t), \theta(t)\} \in \mathcal{R}^- \\ \epsilon^+ + \frac{\sigma(x, t)}{\alpha} - D(p(x, t) - 1) & \text{if } \{p(x, t), \sigma(x, t), \theta(t)\} \in \mathcal{R}^+ \\ \frac{\sigma(t)}{\alpha} - Dp(x, t) & \text{if } \{p(x, t), \sigma(x, t), \theta(t)\} \in \mathcal{R}^a, \end{cases} \tag{2.6}$$

where

$$\begin{aligned} \mathcal{R}^- &= \left\{ \{p, \sigma, \theta\}: \sigma \leq -\gamma p \quad \text{and} \quad (\theta - \theta_0) \leq -\frac{1}{\lambda} \left[B \left(\frac{1}{2} + p \right) - \sigma(\epsilon^- - D) \right] \right\} \\ \mathcal{R}^+ &= \left\{ \{p, \sigma, \theta\}: \sigma \geq -\gamma p \quad \text{and} \quad (\theta - \theta_0) \leq -\frac{1}{\lambda} \left[B \left(\frac{1}{2} - p \right) - \sigma(\epsilon^+ + D) \right] \right\} \\ \mathcal{R}^a &= \left\{ \begin{aligned} & \{p, \sigma, \theta\}: (\theta - \theta_0) \geq -\frac{1}{\lambda} \left[B \left(\frac{1}{2} + p \right) - \sigma(\epsilon^- - D) \right] \\ & \text{and } (\theta - \theta_0) \geq -\frac{1}{\lambda} \left[B \left(\frac{1}{2} - p \right) - \sigma(\epsilon^+ + D) \right] \end{aligned} \right\} \end{aligned} \tag{2.7}$$

and $\gamma = 2B/\epsilon_T$ is defined as in Part I (*cf.* equation (4.4)).

For a fixed σ , the regions \mathcal{R}^- , \mathcal{R}^+ and \mathcal{R}^a are shown in Fig. 1. The θ - p plane is divided into the 3 regions by a horizontal "Y". First look at the low temperatures. Here, we are either in \mathcal{R}^+ or \mathcal{R}^- so according to (2.6), the strains are either close to ϵ^+ or ϵ^- and the material is either in the + variant or - variant of martensite. The exchange of stability takes place when $p = -(1/\gamma)\sigma$, i.e., when $\sigma = -\gamma p$. In other words, at low temperatures, when the stress is above the *Maxwell stress*, the material is in the + variant of martensite and when the stress is below the *Maxwell stress*, the material is in the - variant of martensite. This is exactly as in Part I, Section 4; in particular, the *Maxwell stress* depends on the shift. At high temperature (p, σ, θ) is in the region \mathcal{R}^a , the strains are close to 0 and the material is in the austenite phase. The exchange of stability between the austenite and the two variants of martensite takes place along the two arms of the horizontal Y so that the transformation temperature depends both on the stress and the value of the shift. The slopes of these arms are given by $\pm(\lambda/B)$. The latent heat $\lambda(\theta)$ determines the change of transformation temperature due to both shift and stress, while the parameter B/λ determines the effect of shift on transition temperature at constant stress. Notice that depending on the value of the shift, the austenite loses its stability to one or the other variant of martensite. Finally, the horizontal Y moves up with decreasing σ and down with increasing σ ; it also moves sideways and the direction of the motion depends on the sign of $\sigma(\epsilon^+ + \epsilon^-)$.

We now turn to (2.5)_{ii}. Using (2.2) and (2.6), we obtain

$$\frac{\partial p}{\partial t}(x, t) = \begin{cases} -m(p(x, t) + 1) + d\sigma(x, t) & \text{if } \{p(x, t), \sigma(x, t), \theta(t)\} \in \mathcal{R}^- \\ -m(p(x, t) - 1) + d\sigma(x, t) & \text{if } \{p(x, t), \sigma(x, t), \theta(t)\} \in \mathcal{R}^+ \\ -mp(x, t) + d\sigma(x, t) & \text{if } \{p(x, t), \sigma(x, t), \theta(t)\} \in \mathcal{R}^a \end{cases} \quad (2.8)$$

where $m = \mu B$ and $d = -\mu D$ as in Part I, Section 4.

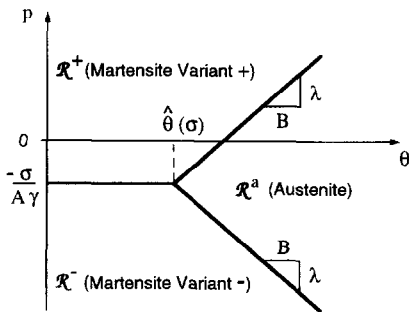


Fig. 1. Regions of stability of the austenite and the "+" and "-" variants of martensite in the σ - p plane. Note that $\hat{\theta}(\sigma) = \theta_0 - (1/2\lambda)[B - \sigma(\epsilon^+ + \epsilon^-)]$.

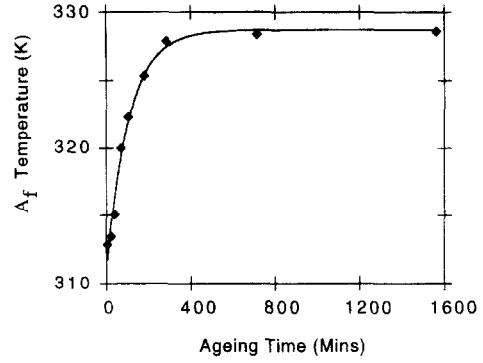


Fig. 2. The stabilization of martensite. The A_f temperature of a bar held in the martensite state rises with holding time. The diamonds show the experimental results extracted from Murakami *et al.* [3], while the curve is the prediction, according to the model and parameters (2.15).

We integrate (2.8) subject to the initial conditions (2.5)_{iii} using a procedure similar to Part I, Section 4. To illustrate, let us fix x and suppress it from the notation. Suppose $\{p_0, \sigma(0), \theta(0)\} \in \mathcal{R}^-$. Therefore, we integrate (2.8)_i to obtain

$$p(t) = p^-(t) = -1 + (p_0 + 1)e^{-m(t-0)} + d \int_0^t \sigma(s)e^{-m(t-s)} ds. \quad (2.9)$$

We continue with this solution until the first time t_1 at which $\{p(t_1), \sigma(t_1), \theta(t_1)\}$ hits the boundary of \mathcal{R}^- . Suppose it hits the boundary between \mathcal{R}^- and \mathcal{R}^+ . At $t = t_1$, we switch to the + branch, (2.8)_{ii}. Integrating (2.8)_{ii} with the initial condition $p^+(t_1) = p(t_1) = p_1$, we get

$$p(t) = p^+(t) = 1 + (p_1 - 1)e^{-m(t-t_1)} + d \int_{t_1}^t \sigma(s)e^{-m(t-s)} ds. \quad (2.10)$$

We continue with this solution until the first time t_2 at which $\{p(t_2), \sigma(t_2), \theta(t_2)\}$ hits the boundary of \mathcal{R}^+ . Suppose it hits the boundary between \mathcal{R}^+ and \mathcal{R}^a . At $t = t_2$, we switch to the austenite branch, (2.8)_{iii}. Integrating (2.8)_{iii} with the initial condition $p^a(t_2) = p(t_2) = p_2$, we get

$$p(t) = p^a(t) = p_2 e^{-m(t-t_2)} + d \int_{t_2}^t \sigma(s)e^{-m(t-s)} ds. \quad (2.11)$$

We continue with this solution until the first time t_3 at which $\{p(t_3), \sigma(t_3), \theta(t_3)\}$ hits the boundary of \mathcal{R}^a . Depending on which boundary it hits, we continue the solution on the relevant branch and so on. We follow an analogous procedure if $\{p_0, \sigma(0), \theta(0)\}$ is in

\mathcal{R}^- or \mathcal{R}^+ . Repeating this procedure for each point x , we obtain $p(x, t)$. Substituting this back in (2.6) we obtain $\epsilon(x, t)$ and then, by integration, the displacement $u(x, t)$.

We now apply this model to a few simple problems.

Stabilization of thermal martensite

Consider a stress-free bar which has been aged in the austenite phase and quenched to a temperature where it completely transforms to the martensite. Suppose it is held at this temperature for a period of time t^* . It has been observed in many common shape-memory alloys subjected to the above treatment that the reverse transformation temperature A_f increases with holding time t^* . In particular, the diamonds in Fig. 2 are the experimental data extracted from Murakami *et al.* [3] in Au-49.5%Cd alloy (note that the composition of this alloy is different from that studied earlier). This phenomenon is called the stabilization of martensite and has important technological implications.

We now examine this problem with our model. We consider a bar with uniform cross-section A in the aged austenite so that the shift $p = 0$ at each point. Before we prescribe initial conditions and applied temperature, let us first examine the transformation temperature $\theta_T(0)$ for this aged bar when the applied stress is zero. Setting $p = 0$, $\sigma = 0$, it is clear from either (2.7) or Fig. 1, that the austenite loses its stability ($\{0, 0, \theta\}$ on \mathcal{R}^0) when the temperature

$$\theta = \theta_T(0) = \theta_0 - \frac{B}{2\lambda}. \quad (2.12)$$

Further, it loses its stability to both variants of martensite. In other words, when $p = 0$, $\sigma = 0$ and $\theta < \theta_T(0)$, both variants of martensite are stable. Thus, on quenching an aged bar, we expect a part l_+ to transform to the + variant of martensite and the remaining part l_- to transform to the - variant.

Therefore, we start with initial data $p_0(x) = 0$, $\epsilon_0(x) = \epsilon^+ + D$ for $x \in l_+$ and $p_0(x) = 0$, $\epsilon_0(x) = \epsilon^- - D$ for $x \in l_-$ corresponding to an aged and quenched bar. The applied stress is zero and the applied temperature is constant at θ_m (where $\theta_m < \theta_T(0)$).

Now, for $t > 0$, we integrate (2.8)_{ii} for $x \in l_+$ and (2.8)_i for $x \in l_-$ to obtain

$$p(x, t) = \begin{cases} p^+(t) = 1 - e^{-mt} & x \in l_+ \\ p^-(t) = -1 + e^{-mt} & x \in l_- \end{cases}. \quad (2.13)$$

Notice that since $\sigma = 0$ and $p^+ > 0$, l_+ continues to remain in the + variant and similarly l_- continues to remain in the - variant.

At time $t = t^*$, the value of the shift has evolved to $p^+(t^*)$ in l_+ and $p^-(t^*)$ in l_- . Therefore, according to (2.7), the transformation temperature changes to

$$\theta = \theta_T(t^*) = \theta_0 - \frac{B}{2\lambda} + \frac{B}{\lambda} (1 - e^{-mt^*}) \quad (2.14)$$

in both parts of the bar. Since $B, \lambda > 0$, the reverse transformation temperature increases with holding time in agreement with experimental observations. (See the paragraph following (2.7) for a discussion of the parameter (B/λ) .) Indeed, for the values

$$\begin{aligned} \theta_0 &= 319.66 \text{ K}, \\ B/\lambda &= 18.12 \text{ K}, \\ m &= 0.009465 \text{ min}^{-1}, \end{aligned} \quad (2.15)$$

we obtain the curve shown in Fig. 2, in good agreement with experimental observations.

Mechanical destabilization of the stabilized thermal martensite

Consider an aged bar of the austenite phase. Suppose it is quenched to a temperature $\theta_m < \theta_0 - B/(2\lambda)$ where it completely transforms to a mixture of martensite variants. Suppose it is held at that temperature at zero load for time t^* . As we have seen above, the martensite begins to stabilize as the shift evolves according to (2.13) to $p^+(t^*)$ in l_+ (the part of the bar that transforms to the + variant) and $p^-(t^*)$ in l_- . Furthermore, as we have seen in (2.14), the reverse transformation temperature rises to $\theta_T(t^*)$ indicating a stabilization of the martensite.

Suppose at time $t = t^*$, we begin to apply a sinusoidal load $F(t) = F_0 \sin(\omega(t - t^*))$ (with F_0 chosen large enough to detwin the bar), while still maintaining the temperature constant at θ_m . Since the temperature is constant below the transformation temperature, we involve only the two variants of martensite. In other words, for $t > t^*$, this problem is exactly the one studied extensively in Part I, Section 4. It is clear from Fig. 4 there that with increasing cycles of the applied load, the value of the shift in both parts l_+ and l_- of the bar begins to approach zero and after a sufficiently large number of loading cycles, the shift is very close to zero in the entire bar. Therefore, after this loading, the (reverse) transformation temperature is going to be close to $\theta_T(0)$ (the transformation temperature of aged austenite) which is smaller than $\theta_T(t^*)$. Thus, by applying a sinusoidal loading, we have been able to decrease the transformation temperature, i.e., we have been able to (mechanically) destabilize the (thermally) stabilized martensite.

Let us discuss this prediction in the light of our one-dimensional hypothesis. First note that in a full three-dimensional theory, which is difficult to construct at this time because of the lack of knowledge of the precise mechanism, we would need to allow for vector-valued shifts. Then it is not clear that cycling between two variants of martensite would cause the shift to evolve to the preferred value of the austenite. However, symmetry considerations suggest that qualitative aspects of this prediction should still be true. If, as is the case in many martensitic transformations, the point group of the martensite is a subgroup of that of the austenite, then,

the preferred values of the shifts for the different variants of martensite are likely to be related by the action of this group. If the austenite has cubic symmetry, for example, this implies that the preferred values of the shifts for the different variants of martensite lie on the corners of a regular polyhedron centered at the origin, while the preferred shift for austenite is zero. Furthermore, cycling between two variants would cause the shift to evolve to an average value which would be closer to the center (preferred value of austenite) than the corners. Thus we expect that during cycling the shift will evolve toward the preferred value(s) for austenite and, consequently, the transformation temperature should decrease, though not possibly to the value for aged austenite. Hence, measurements of the three temperatures: $\theta_T(0)$, $\theta_T(t^*)$ and the transformation temperature just after extensive cycling of the martensite, will provide indirect information about the mechanism; if the two latter temperatures are nearly equal, it suggests that the ordering or shuffle that develops after long term cycling of the martensite is close to that of the aged austenite.

Based on these considerations, we suggest this as an experiment to examine whether the mechanism responsible for the stabilization of martensite is the same one responsible for the rubber-like behavior.

Stabilization of stress-induced martensite

Consider a bar with uniform cross-section A aged in the austenite state. Suppose we continue to hold this bar at a constant temperature above the transformation temperature and subject it to an applied stress σ^* large enough so that the bar fully transforms to the martensite. We hold this load for time t^* and seek the state of the bar. In particular, we seek to know if the bar would revert to the austenite when unloaded; if so, we seek the value of applied stress at which the reverse transformation takes place. Finally, if the bar is unloaded at time t^* and reverts to the austenite, we seek the temperature at which it would transform to the martensite on sudden cooling.

Before we prescribe the initial data, let us examine the transformation stress for a bar aged in the austenite state. We take $p = 0$ and applied temperature $\theta > \theta_T(0) = \theta_0 - (B/2\lambda)$ (cf. (2.12)). For these values, it follows from (2.7) that the austenite transforms to + and - variants at the stress

$$\sigma^+(0) = \frac{\lambda}{(\epsilon^+ + D)} \left\{ \theta - \left(\theta_0 - \frac{B}{2\lambda} \right) \right\}$$

and

$$\sigma^-(0) = \frac{\lambda}{(\epsilon^- - D)} \left\{ \theta - \left(\theta_0 - \frac{B}{2\lambda} \right) \right\}, \quad (2.16)$$

respectively. Since we have assumed that $\epsilon^+ > 0 > \epsilon^-$ and $|D| \ll |\epsilon^+|, |\epsilon^-|$, we have that $\sigma^+(0) > 0 > \sigma^-(0)$.

In other words, if we apply a tensile stress larger than $\sigma^+(0)$, the austenite transforms to the + variant while if we apply a compressive stress larger than $|\sigma^-(0)|$, the austenite transforms to the - variant. In particular, we note the interesting relationship

$$\sigma^+(0)\epsilon^+ \approx \sigma^-(0)\epsilon^-. \quad (2.17)$$

We note in passing that in this one-dimensional theory, there is no kinematic compatibility. In three dimensions, kinematic compatibility (written as the crystallographic theory of martensite, for example) would prevent the austenite from transforming to a single variant of martensite. So in reality we would expect the austenite to transform to a mixture of the two variants and then to a single variant. In any case, what (2.16) says is that it is possible to stress-induce the martensite and that the + and - variants are stable when we apply sufficiently large tensile and compressive stresses respectively.

We now return to the problem of the bar aged in austenite. We apply a constant temperature $\theta > \theta_0 - (B/2\lambda)$ and a constant applied stress $\sigma^* > \sigma^+(0)$. We choose initial data $p_0 = 0$, $\epsilon_0 = \epsilon^+ + \sigma^*/\alpha + D$ for each x in the bar corresponding to aged austenite freshly transformed to the + variant of martensite under the action of the applied stress. For time $t > 0$, $p(x, t)$ evolves according to equation (2.8)_i (which corresponds to the + variant). Integrating it with the initial condition $p_0 = 0$, we find that for each x in the bar,

$$\begin{aligned} p(x, t) &= p^*(t) = 1 + (0 - 1)e^{-mt} \\ &+ \int_0^t \sigma(s)e^{-m(t-s)} ds \\ &= \left(1 - \frac{D\sigma^*}{B} \right) (1 - e^{-mt}). \end{aligned} \quad (2.18)$$

At time $t = t^*$, the shift has evolved to the value $p^*(t^*)$ and consequently according to (2.7), the stress for reverse transformation is given by

$$\begin{aligned} \sigma^+(t^*) &= \frac{\lambda}{(\epsilon^+ + D)} \left\{ \theta - \left(\theta_0 - \frac{B}{2\lambda} \right) \right\} \\ &- \frac{B}{(\epsilon^+ + D)} \left(1 - \frac{D\sigma^*}{B} \right) (1 - e^{-mt^*}). \end{aligned} \quad (2.19)$$

Thus, we see that stress for reverse transformation $\sigma^+(t^*)$ changes exponentially with holding time. Further, the stress may increase or decrease depending on the value of $(1 - D\sigma^*/B)$. In particular, if $D \leq 0$, the stress increases with holding time.

Finally suppose the bar is unloaded at time $t = t^*$ and reverts to the austenite. We examine the transformation temperature if the bar is suddenly cooled at time $t = t^* +$. Since the value of the shift is given by $p^*(t^*)$, the transformation temperature

changes to

$$\theta = \theta_T(t^*) = \theta_0 - \frac{B}{2\lambda} + \frac{B}{\lambda} (1 - D\sigma^*/B)(1 - e^{-mt^*}). \quad (2.20)$$

Thus, depending on the sign of D and the magnitude of the applied load, the stress-induced martensite is either stabilized or destabilized. This is a key difference compared with the thermal martensite where the martensite is always stabilized (*cf.* (2.14)).

3. PROPOSALS FOR NEW EXPERIMENTS

In this section, we propose some new experiments to (a) critically examine our theory and (b) to use our theory to explore the mechanism responsible for the relaxation.

Mechanical tests

Lieberman *et al.* [2] were interested in the behavior of the material under both tension and compression. Consequently, they were forced to use a severely nonuniform cross-section in order to prevent buckling. Further, they measured the diametral strain and converted it to actual strain. Unfortunately, this introduces various complications in extracting reliable material parameters. Therefore, we propose using a specimen with uniform cross-section. The loading programs below are limited to tension; so buckling is not a concern. Further, we suggest that the actual extension be measured directly using a suitable extensometer.

Consider a single crystal bar of austenite. Cool it carefully to transform it to the martensite using a single austenite–martensite interface to obtain a fairly uniform distribution of fine twins of two variants of martensite. Age the bar in this state and then subject it to the various experiments described below. It is important to start each experiment with an aged finely twinned bar.

1. *Load–hold–unload.* We begin with a very simple experiment in order to determine the material parameters: α , B , D , ϵ_T , $m = \mu B$, σ_{xs} . First measure

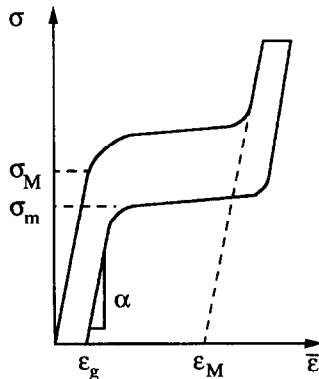


Fig. 3. A schematic hysteresis loop (stress vs overall strain) during the load–hold–unload test.

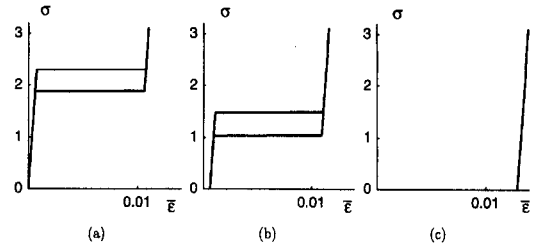


Fig. 4. Simulated hysteresis (stress vs overall strain) with loading (3.2) with $F_0/A = 3.1$ and $\omega = 7.5 \times 10^{-2}$ Hz and material parameters (3.3). (a) Initial loop, (b) loop after 100 cycles (c) terminal loop after 1000 cycles.

the volume fractions of the two variants in the aged finely twinned bar. Apply a tensile load large enough so that one of the two variants (the one with initial volume fraction λ) completely disappears. Hold the load constant at this value for a time t^* and then unload to zero. Repeat this experiment with different holding times, taking care to start with an aged bar on each occasion.

We expect to obtain a hysteresis loop of the type shown schematically in Fig. 3. We expect α , σ_M , ϵ_M to remain constant independent of holding time t^* , while σ_m and ϵ_g are expected to change with holding time t^* . The parameters may be obtained from the following formulas:

$$\begin{aligned} \epsilon_T &= \epsilon_M/\lambda, \\ \sigma_{xs} &= (\sigma_M - \sigma_m|_{t^*=0})/2, \\ B &= \epsilon_T(\sigma_M - \sigma_{xs})/2, \end{aligned} \quad (3.1)$$

$$\sigma_m = c_1 + c_2 e^{-\mu B t^*} \quad \text{for some constants } c_1 \text{ and } c_2,$$

$$\epsilon_g = \left(\frac{D\sigma^*}{B} + 2\lambda \right) (1 - e^{-\mu B t^*}).$$

The first three equations give ϵ_T , σ_{xs} , B respectively, the fourth gives $m = -\mu B$, and the fifth gives D .

2. *Tension cycle.* Apply a load

$$F(t) = F_0 |\sin(2\pi\omega t)| \quad (3.2)$$

for $F_0 > [(B/\epsilon_T) + \sigma_{xs}]A$ where A is the cross-sectional area of the bar (since we will plot only stress, we do not need the value of A).

In the initial cycles, our model predicts a hysteresis loop like the one shown in Fig. 4(a). With cycling, the hysteresis loop begins to come down as in Fig. 4(b). After a sufficient number of cycles, the hysteresis loop completely disappears and the bar behaves almost like a linear elastic bar as shown in Fig. 4(c). These curves were simulated using the parameters

$$\begin{aligned} \alpha &= 3000 \text{ kg/mm}^2, \\ B &= 0.017 \text{ kg/mm}^2, \\ D &= -0.003 \text{ kg/mm}^2, \end{aligned} \quad (3.3)$$

$$\epsilon_T = 0.02,$$

$$\begin{aligned}\sigma_{xs} &= 0.2 \text{ kg/mm}^2, \\ \mu &= 0.8 \text{ mm}^2/(\text{kg min}),\end{aligned}$$

which are the same as those for equation (6.3) in Part I. Clearly, the experimental results must be compared with curves simulated using the parameters determined by the load–hold–unload experiment and (3.1).

Once the bar is in the terminal loop, stop the loading at zero load and hold for time t^* . Then resume the loading (3.2). Our models predict that the stress–strain curves will remain similar to the collapsed terminal loop shown in Fig. 4(c); if the parameter D is negative (as suggested by the experiments of Lieberman *et al.*), the stress–strain curve will shift slightly to the left. In any case, our model predicts that under the tensile loading (3.2), there will *not* be any recovery like that observed by Lieberman *et al.* [2] (see Fig. 1 of Part I).

Repeat the experiment of tensile cycling of an aged finely twinned bar at different temperatures as well as different frequencies and amplitudes of loading. Our model predicts that the hysteresis loops will qualitatively look similar to those shown in Fig. 4. The width of the initial hysteresis loop is predicted to increase with increasing temperature, decreasing frequency and increasing amplitude (this last prediction will be true if the material parameter $D < 0$, but will be reversed if $D > 0$).

3. Unusual tension cycle. Apply a load

$$F(t) = \begin{cases} F_0 \sin(2\pi\omega t) & \text{if } \frac{n}{\omega} \leq t < \frac{3n+1}{3\omega}, \\ 0 & \text{if } \frac{3n+1}{3\omega} \leq t < \frac{3n+3}{3\omega} \end{cases} \quad n = 0, 1, \dots \quad (3.4)$$

for some $F_0 > [(B/\epsilon_T) + \sigma_{xs}]A$ where A is the cross-sectional area of the bar. This loading cycle consists of a tension cycle of duration $1/3\omega$ followed by a hold at zero load for a duration of $2/3\omega$.

In the initial cycles, our model predicts a hysteresis loop like the one shown in Fig. 5(a). With cycling, the hysteresis loop begins to come down as in Fig. 5(b). However, unlike Fig. 4, the hysteresis loop does not

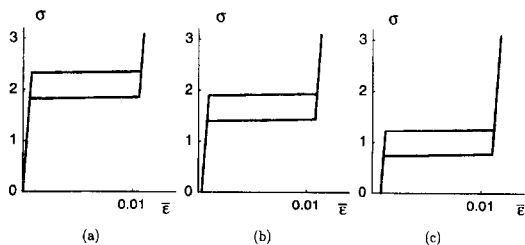


Fig. 5. Simulated hysteresis loops (stress vs overall strain) with loading (3.4) with $F_0/A = 3.1$ and $\omega = 7.5 \times 10^{-2}$ Hz and material parameters (3.3). (a) Initial loop, (b) loop after 200 cycles and (c) terminal loop after 1000 cycles.

completely disappear; instead it attains the terminal loop as shown in Fig. 5(c). Further cycling does not cause any changes. Note that these figures were generated using parameters (3.3). Clearly, the experimental results must be compared with curves simulated using the parameters determined by the load–hold–unload experiment and (3.1).

Once the bar is in the terminal loop, stop the loading at zero load and hold for time t^* . Then resume the loading (3.3). Our models predict that with increasing holding time t^* , the hysteresis loop gradually recovers, in contrast with the previous experiment; with sufficiently long holding time it completely goes back to the initial loop.

4. *Effect of orientation.* Repeat Experiment 1, load–hold–unload for specimens with different orientation and determine how the parameters depend on orientation. It is likely that different mechanisms of relaxation will predict different orientation dependence of the parameters. This information may prove crucial for testing different mechanisms, and would provide useful guidelines for the development of 3D shift relaxation models.

Thermal and combined thermal–mechanical tests

An important question is whether the mechanisms responsible for the rubber-like behavior and stabilization of martensite are the same. In Section 2, we presented a theory assuming that they were the *same*.

Based on this theory we proposed and predicted the results of three sets of experiments; we collect them here.

5. *Stabilization of thermal martensite.* Consider a single crystal bar of austenite. Cool it until it completely transforms to martensite. Hold it in the martensite for time t^* . Heat it and measure the temperature at which it transforms to the austenite (either A_s or A_f will do as long as it is used consistently). Repeat the experiment with different holding times. We expect that the transformation temperature will increase with t^* according to the relation (2.14). From the data, we can easily obtain B/λ and m . From an independent measurement of latent heat λ we can obtain the parameters B and $\mu = m/B$. Compare these values with the values obtained from the mechanical tests (3.1). If they are similar, then the mechanisms responsible for the rubber-like behavior and stabilization of martensite are likely to be the same. On the other hand, if they are not similar, it is a strong evidence that the mechanisms are different.

6. *Mechanical destabilization of the stabilized thermal martensite.* Consider a single crystal bar of austenite. Cool it until it completely transforms to martensite. Hold it in an unloaded state in the martensite for time t^* . At time $t = t^*$, subject the bar to a sinusoidal tension-compression loading cycle similar to those considered by Lieberman *et al.* [2] and considered in length in Sections 4, 5 and 6 of Part I. Notice that this experiment may require care to prevent buckling. Initially the hysteresis response will be a double loop; with cycling it will evolve to the terminal single loop. Once the specimen attains the terminal loop, stop the loading and heat until it transforms to the austenite and measure the transformation temperature. Our one-dimensional model predicts that the transformation temperature will be independent of the holding time t^* ; however, as we noted in Section 2, this prediction may depend crucially on the exact three-dimensional nature of the mechanism and the underlying material symmetry. Therefore, this experiment may provide critical information about the nature of the exact mechanism.

7. *Stabilization of stress-induced martensite.* Consider a single crystal bar of austenite. Apply a tensile load until it fully transforms to the martensite. Hold the load for a time t^* and then unload. Measure the value of the load at which it transforms back to the austenite. Our model predicts that this will depend on the holding time according to (2.19); therefore we can estimate the coupling parameter D and contrast it with that obtained from the purely mechanical tests.

4. CONCLUSION AND DISCUSSION

A wide variety of relaxation phenomena like the stabilization of martensite and rubber-like behavior are known to occur in common shape-memory alloys. These phenomena adversely affect applications. There is a great wealth of experimental data; yet there is no agreement on the exact mechanism. However, there is a broad consensus that "the free energy per unit volume in the region swept by the moving twin boundary is temporarily increased but may be decreased again by some thermally activated relaxation process" (Christian [4]).

We have proposed a phenomenological, but predictive, model of the behavior of these materials based on this point of view. The basic model was presented in Part I and extended to include temperature in Section 2 of this part. The model is one-dimensional and is based on an energy which depends on strain and an internal variable which we call shift. Section 2 of Part I presents one concrete interpretation of the shift based on the mechanism proposed by Lieberman *et al.* [2]. However, it is possible to obtain similar interpretations for other mechanisms, such as short-range order. The principal

assumption of the model is that the material has a few energetically preferred states, with each preferred state characterized by a preferred strain and shift. Second, the relaxation of the shift is assumed to be much slower than the attainment of elastic equilibrium, so that kinetics is dominated by the shift relaxation. Third, the shift evolves by gradient-flow kinetics on this multi-welled energy. We write down equations based on these ideas and solve them given the initial state, applied load and temperature history. All the parameters in our model are easily determinable and held fixed during the simulations. Further, our model does not incorporate any *ad hoc* criterion to obtain the hysteresis or its evolution. They all follow from the basic equations.

In Section 6 of Part I, we show that the results of our simulations compare favorably with the experimental observations of Lieberman *et al.* [2]. Our model is able to capture all the qualitative features of the wide range of experiments. Further, we also found quantitative agreement wherever such a comparison was possible; unfortunately, given the nature of the available experimental data, detailed quantitative investigation of the model was not possible. In Section 2, we simulated some experiments on the stabilization of martensite to find good qualitative and quantitative agreement.

We can therefore conclude that the simple statement of Christian, together with some easily measured material constants, is sufficient to predict many aspects of the behavior of these alloys.

In Section 3 of this part, we have proposed new experiments for two purposes. The first is to provide definitive quantitative tests for this model. The second and more important purpose is to use this model to further investigate the mechanisms responsible for these relaxation mechanism.

Acknowledgements—We gratefully acknowledge many useful and colorful discussions with David Lieberman. Part of this work was conducted when K.B. and P.J.S. held post-doctoral positions at the Courant Institute. This work was partially supported through grants from the AFOSR (KB, PJS:90-0090 at Courant, KB:F49620-95-1-0109 at Caltech, RDJ:91-0301), ARO(KB:DAAL03-92-G-0011 at Courant, PJS:DAAH04-95-1-0100 at Courant), DOE(PJS:W-7405-ENG-36 and KC-07-01-01), NSF(RDJ:DMS-9505077, PJS:DMS-9402763 at Courant), and ONR (KB:N00014-93-1-0240 at Caltech, RDJ:N/N00014-95-1-1145 and 91-J-4304).

REFERENCES

1. Bhattacharya, K., James, R. D. and Swart, P. J., *Acta Mat.*
2. Lieberman, D. S., Schmerling, M. A. and Karz, R. S., in *Shape Memory Effect in Alloys*, ed. J. Perkins, Plenum Press, New York, 1975, pp. 203–242.
3. Murakami, Y., Morito, S., Nakajima, Y., Otsuka, K., Suzuki, T. and Ohba, T., *Mater. Lett.*, 1994, **21**, 275.
4. Christian, J. W., *Metall. Trans. A*, 1982, **13A**, 509.